PHYSICAL REVIEW B VOLUME 46, NUMBER 24 15 DECEMBER 1992-II

High-energy electron transport

Luo Zhengming
Center for Radiation Physics, Institute of Nuclear Science and Technology, Sichuan University, Chengdu, People's Republic of China

Anders Brahme
Department of Radiation Physics, Karolinska Institutet and Stockholm University, Box 60211, S-10401 Stockholm, Sweden
(Received 14 May 1992)

The bipartition model for electron transport has been extended to the energy range from 1 to 50 MeV because of its importance for radiation therapy. In the extended version, the influence of energy-loss straggling, secondary-electron production, and bremsstrahlung production on electron transport has been included. In addition, the transport of obliquely incident electrons has also been considered. The extended theory is described in detail and computational results including the electron-energy deposition, the charge deposition, and the angular distribution are given. Compared with the Monte Carlo method, the extended bipartition theory shows a much higher computational efficiency, while retaining a high precision. Moreover, comparisons between the moment method and the bipartition model demonstrate also that the latter possesses higher precision and flexibility.

I. INTRODUCTION

The practice of modern radiation therapy calls for fast calculations of high-energy-electron transport in the human body. Such energy-deposition calculations are especially important for high-energy accelerators used in radiation therapy.

During the early 1970s, Kessaris extended the use of the moment method proposed by Spencer to treat the problem of high-energy-electron transport in water for medical applications.[1,2] The results obtained by using the moment method were in reasonable agreement with experimental data. Due to the adoption of the continuous-slowing-down approximation (CSDA), however, some factors, such as energy-loss straggling which is important for high-energy-electron transport, were not considered in Kessaris's work. Moreover, with the moment method it is difficult to treat the electron transport with oblique incidence and semi-infinite or multilayer media. Brahme and Jette extended the Fermi-Eyges small-angle multiple-scattering theory to calculate the energy deposition of high-energy electrons in water.[3-6] The method of Hogstrom, Mills, and Almond and Brahme, Lax, and Andreo has been used widely in clinical practice.[7,8] However, as pointed out by these authors, the Fermi-Eyges theory needs to be improved, especially for the transport with inhomogeneities and at large depth. Recently Huizenga and Storchi have used the phase-space time-evolution method to treat the transport calculation for high-energy electrons and have shown good results.[9,10] Until now, the most accurate method for calculation of the electron penetration might be the Monte Carlo method. Berger and Seltzer, Halbleib and Van-devender, Nelson, Hirayama, and Rogers, and Andreo and Brahme have developed different codes of Monte Carlo calculation.[11-14] The Monte Carlo method can simulate not only the electron transport process in detail, but also its calculational efficiency, which has largely been improved. Generally, Monte Carlo simulation has satisfied the main requirements largely for the electron transport calculation for medical applications, except for its slow calculational efficiency.

The bipartition model of electron transport has shown high quality in the description of the electron transport within the energy range 20 keV–1 MeV with high calculation precision, flexibility, and efficiency.[15,16] In this paper, we will extend the model to handle the transport of 1–50-MeV electrons in water. For high-energy electrons, some other factors have to be considered. These factors include energy-loss straggling, secondary-electron transport, and bremsstrahlung. We have therefore completed another version of the MONKEY program, MONKEY.RT, which is capable of handling the transport of 1–50-MeV electrons in water. The MONKEY.RT code shows very high computational efficiency, and still keeps good calculation quality. This fact implies that it may become a promising way to employ the bipartition model for the calculation of electron transport in media.

There are five sections in this paper. After a brief formulation of the electron-atom interaction process, we introduce the extended bipartition model in detail. In the fourth section, we present results computed by the MONKEY.RT code. Some of the results are compared with more detailed Monte Carlo simulations, the moment method results, and experimental data. The last section is a brief discussion of the results.

II. FUNDAMENTALS OF THE INTERACTION OF ELECTRONS WITH ATOMS

The electron-energy range considered in this paper is approximately 1–50 MeV. Within this range, four principal interactions of the electrons with matter have been taken into account in the Boltzmann equation: the total

electron stopping power, the energy-loss straggling, the bremsstrahlung cross section, and the elastic-scattering cross section.

The electron stopping power, giving the average energy loss of electrons passing through a unit depth interval, is normally expressed by the Bethe-Block equation.[17] A more perfect stopping power formula should also take bremsstrahlung, density effect, and shell correction into consideration. In order to consider the transport of secondary electrons in the medium, the restricted collision stopping power has to be used:

$$L(E,\Delta)=\frac{N_A ZD}{A}m_0c^2\frac{2\pi r_0^2}{\beta^2}[2\ln(E/I)+\ln(1+E/2)+G(E,\Delta)-\delta-2C/Z] . \tag{1}$$

When $\Delta=E/2$, $L(E,\Delta)$ becomes the conventional collision stopping power. The radiation stopping power is[18]

$$S_{\rm rad}(E)=\frac{N_A D}{A}Z(Z+1)\frac{r_0^2}{137}(E+m_0c^2)\varphi_{\rm rad} . \tag{2}$$

In the present calculations, the fitting formula for $\varphi_{\rm rad}$ given by Seltzer and Berger[19] has been used.

The function $G(E,\Delta)$, by definition, is given by

$$G(E,\Delta)=-1-\beta^2+\ln\left[4\frac{\Delta}{E}\left[1-\frac{\Delta}{E}\right]\right]+\left[1-\frac{\Delta}{E}\right]^{-1}+(1-\beta^2)\left[\frac{\Delta^2}{2(m_0c^2)^2}+\left[\frac{2E}{m_0c^2}+1\right]\ln\left[1-\frac{\Delta}{E}\right]\right] . \tag{3}$$

The total stopping power is

$$\rho_t(E)=L(E,E/2)+S_{\rm rad}(E) , \tag{4}$$

where N_A is Avogadro's number, and Z and A are the atomic number and atomic weight of the atom, respectively. r_0 is the classical electron radius, I is the average ionization potential, δ is the density effect correction, and $2C/Z$ is the shell correction factor. D is the density for the medium. From Eq. (4) the CSDA electron range is given by

$$R(E)=\int_0^E dE'/\rho_t(E') . \tag{5}$$

In order to include energy-loss straggling in the calculations, the energy-loss straggling factor Ω_t is needed. By definition, the factor Ω_t is made up of its collision and radiation parts,

$$\Omega_t=\Omega_c+\Omega_r , \tag{6}$$

where

$$\Omega_c=\frac{N_A Z}{A}D\int_0^{E/2}\sigma_M(E,T)T^2\,dT \tag{7}$$

$$\approx\frac{N_A Z}{A}D\frac{2\pi r_0^2 m_0c^2}{\beta^2}E\left[2-2\ln 2+\frac{1}{24}\frac{E^2}{(E+m_0c^2)^2}-\frac{m_0c^2(2E+m_0c^2)}{(E+m_0c^2)^2}(\ln 2-0.5)\right] , \tag{8}$$

$$\Omega_r=\frac{N_A D}{A}\int_0^E\sigma_r(E,T)T^2\,dT \tag{9}$$

$$\approx(\alpha_1+\alpha_2E^{\alpha_3})ES_{\rm rad} , \tag{10}$$

where σ_M is the Moller cross section and σ_r is the bremsstrahlung cross-section differential in photon energy. $\alpha_1=0.3000$, $\alpha_2=0.022\,26$, $\alpha_3=0.356\,55$ for water. T is the energy transfer in units of megaelectron volts.

In the extended model not only the radiation stopping power and its straggling parameter are needed, but also the bremsstrahlung cross-section differential in energy is needed. The bremsstrahlung cross section given in Ref. 20 is

$$\frac{d\sigma}{dT}=\frac{4r_0^2Z^2}{137T}\left[\left[1+\frac{(E-T)^2}{E^2}-\frac{2}{3}\frac{E-T}{E}\right]\left[\frac{\Phi_1(\gamma)}{4}-\tfrac{1}{3}\ln Z\right]+\frac{E-T}{6E}\Delta(\gamma)\right] , \tag{11}$$

$$\gamma=100\frac{m_0c^2T}{E(E-T)Z^{1/3}} .$$

We give the formulas for the functions $\Phi_1(\gamma)$ and $\Delta(\gamma)$ fitted over the relevant range of γ:

$$\Phi_1(\gamma)=a_1e^{-a_2\gamma}+b_1e^{-b_2\gamma}, \tag{12}$$

$$\Delta(\gamma)=\Phi_1-\Phi_2=c_1e^{-c_2\gamma}+d_1e^{-d_2\gamma}, \tag{13}$$

where $a_1=6.892$, $a_2=0.4813$, $b_1=13.817$, $b_2=0.032\,89$, $c_1=0.2592$, $c_2=2.869$, $d_1=13.817$, $d_2=0.032\,89$.

The elastic-scattering cross section of an electron in a Coulomb field has been deduced by Rutherford by means of classical mechanics. However, for a more accurate scattering cross-section formula, the following three factors must be considered: the screening effect on the electric field of the nuclei resulting from the electron cloud outside nuclei, the inelastic scattering, and the relativistic effect. In our calculation, the above three factors have been taken into consideration. Because water is a typical medium in our calculation, the McKinley-Feshbach formula for elastic electron scattering has been used.[21] The formula is

$$\sigma_{\rm MF}(E,\theta)=r_0^2Z(Z+1)(m_0c^2)^2(E+m_0c^2)^2/E^2(E+2m_0c^2)^2\left[\frac{1}{(1+2\eta-\cos\theta)^2}+\frac{\pi\beta}{\sqrt{2}}\frac{Z}{137}(1-\cos\theta)^{-3/2}-\frac{1}{2}\left[\beta^2+\frac{\pi\beta Z}{137}\right](1-\cos\theta)^{-1}\right]. \tag{14}$$

Here

$$\eta=\frac{1}{4}\left[\frac{Z^{1/3}}{121.25}\right]^2\left[1.13+3.76\left[\frac{Z}{137}\right]^2\frac{(E+m_0c^2)^2}{E(E+2m_0c^2)}\right]\frac{(m_0c^2)^2}{E(E+2m_0c^2)}. \tag{15}$$

η is the Moliere screen factor.[22] In the calculations we shall apply the following scattering coefficient:

$$\varphi_l(E)=2\pi\frac{N_A}{A}D\int_{-1}^{1}[1-p_l(\mu)]\sigma_{\rm MF}(E,\theta)d\mu. \tag{16}$$

Using Eq. (14), we have

$$\varphi_l(E)=\frac{N_A}{A}DZ(Z+1)2\pi r_0^2\frac{(E+m_0c^2)^2(m_0c^2)^2}{E^2(E+2m_0c^2)^2}\left[C_l+2\pi\alpha\beta l-(\beta^2+\pi\alpha\beta)\sum_{i=1}^{l}i^{-1}\right] \tag{17}$$

and the recursion formula for C_l becomes

$$\begin{aligned}&C_0=0,\\&C_1=\ln(1+1/\eta)-(1+\eta)^{-1},\\&C_{l+1}=(2+1/l)(1+2\eta)C_l-(1+1/l)C_{l-1}-(2+1/l)/(1+\eta).\end{aligned} \tag{18}$$

III. THE EXTENDED BIPARTITION MODEL FOR ELECTRON TRANSPORT

The bipartition model of electron transport under the CSD assumption has been verified to be successful for describing the transport of 10-keV to 1-MeV electrons. When one tries to extend the theory to a wider energy range, other factors must be considered. Primarily, the energy-loss straggling and secondary-electron transport have to be considered to obtain accurate absorbed dose distributions. The transport of the remaining electron after bremsstrahlung emission should also be treated in more detail.

A. The primary-electron transport including energy-loss straggling and the bremsstrahlung process

Assuming that an infinitely wide electron beam is incident upon the surface of a homogeneous semi-infinite solid, the entrance side of the surface may be either the same medium or vacuum. Selecting the x axis along the normal direction of the surface of the solid with the origin on the surface, the Boltzmann equation within the Fokker-Planck frame is given by[15]

$$-\frac{\partial\rho_c f}{\partial E}+\mu\frac{\partial f}{\partial x}-\frac{1}{2}\frac{\partial^2}{\partial E^2}(\Omega_c f)+\varphi_r f=C_f(x,\mu,E)+\left[\frac{N_AD}{A}\right]\int_E^{E_0}dE'\,f(x,\mu,E')\sigma_r(E',E'-E)+\delta(x)\delta(1-\mu)\delta(E-E_0)/2\pi, \tag{19}$$

$$C_f(x,\mu,E)=\int_{4\pi}d\mathbf{u}'[f(x,\mu',E)-f(x,\mu,E)]\frac{N_A}{A}D\sigma_{\rm MF}(E,\mathbf{u}\cdot\mathbf{u}'), \tag{20}$$

$$\varphi_r(E)=\frac{N_AD}{A}\int_\varepsilon^E\sigma_r(E,T)dT.$$

Here $f(x,\mu,E)$ is the electron fluence differential in angle and energy E of the electrons. μ is the cosine of the angle between the electron direction $\mathbf{u}$ and the x axis. $\rho_c=L(E,\Delta)$, φ_r is the total cross section of bremsstrahlung. In order to describe the transport of high-energy electrons in water accurately the influence of bremsstrahlung has to be considered in detail. This is because bremsstrahlung, on the one hand, contributes to an increasingly important part of the stopping power of electrons with increasing electron energy and, on the other hand, the influence of bremsstrahlung upon electron transport differs from inelastic collisions. Having emitted a bremsstrahlung photon, the energy spread of the electron is much larger than that for elastic collisions. In this way, we assume that, having emitted a bremsstrahlung photon, both the forward-directed electrons and the diffusion electrons belong to the diffusion electron component. Furthermore, we have neglected the events when the electrons emit photons with low energy. In so doing, first of all we may avoid the divergent difficulty of the total bremsstrahlung cross section. Second, the approximation appears to be reasonable, because the influence of such events on electron transport is very weak. In our calculation we neglect the event of emitting a photon with energy lower than $\varepsilon=0.02E_0$. Besides, due to the small deflection of recoil electrons we neglect the directional change after an electron emitted photon. The first term of the right side of Eq. (19) is represented by C_f, called the scattering integral, which represents the net increase in the number of electrons per unit solid angle in direction $\mathbf{u}$, passing through a unit distance caused by elastic scattering. Obviously

$$\int_{4\pi} C_f(x,\mu,E)d\mathbf{u}=0 \ . \tag{21}$$

Equation (21) shows that the elastic scattering only gives rise to the change of electron angular distribution. From Eq. (21) and the property that the small-angle elastic scattering of electrons is dominating, the main characteristics of C_f can be estimated, as shown in Fig. 1. According to the bipartition model of electron transport, the scattering integral is divided into two parts, of which one is the comparatively isotropic diffusion electron source S_d, which includes nearly all the large-angle scattered electrons; the other is the remaining part that spreads mainly in the forward small-angle directions. The latter remaining part is normally of negative value, demonstrating that the number of electrons that leave the forward small-angle direction due to elastic scattering is larger than that of the electrons that enter the small-angle directions caused by elastic scattering. Following the bipartition model, the total distribution function $f(x,\mu,E)$ is formed by the distribution function of forward-directed electrons $f_s(x,\mu,E)$ and the distribution function of diffusion electrons $f_d(x,\mu,E)$. According to

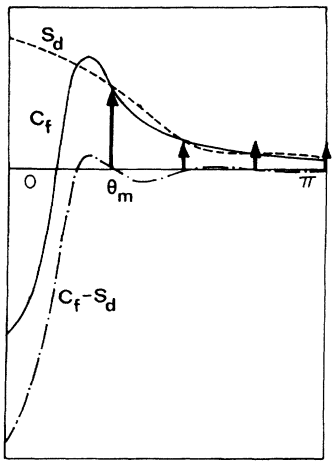

FIG. 1. An illustration of the scattering integral and partition condition. $\theta_{\min}$ is the smallest selected large angle which can be used for determining diffusion electron source. The arrows show the selected large angle for partition condition. The solid line is the scattering integral. The dashed line is the diffusion electron source S_d, and the dashed-dotted line is the rest part of the scattering integral which still belongs to the forward-directed electrons having moved the rather isotropic portion from the scattering integral to diffusion electrons.

$$f(x,\mu,E)=f_s(x,\mu,E)+f_d(x,\mu,E) \ , \tag{22}$$

the Boltzmann equation can be composed into two subequations coupled to each other:

$$-\frac{\partial\rho_c f_s}{\partial E}+\mu\frac{\partial f_s}{\partial x}-\frac{1}{2}\frac{\partial^2}{\partial E^2}(\Omega_c f_s)+\varphi_r f_s=\frac{N_A}{A}D\int_{4\pi}d\mathbf{u}'[f_s(x,\mu',E)-f_s(x,\mu,E)]\sigma_{\mathrm{MF}}(E,\mathbf{u}'\cdot\mathbf{u})$$
$$-S_d+\delta(x)\delta(1-\mu)\delta(E-E_0)/2\pi \ , \tag{23}$$

$$-\frac{\partial\rho_c f_d}{\partial E}+\mu\frac{\partial f_d}{\partial x}-\frac{1}{2}\frac{\partial^2}{\partial E^2}(\Omega_c f_d)+\varphi_r f_d=\frac{N_A}{A}D\int_{4\pi}d\mathbf{u}'[f_d(x,\mu',E)-f_d(x,\mu,E)]\sigma_{\mathrm{MF}}(E,\mathbf{u}\cdot\mathbf{u}')$$
$$+\frac{N_A}{A}D\int_{E+\varepsilon}^{E_0}dE'[f_s(x,\mu,E')+f_d(x,\mu,E')]\sigma_r(E',E'-E)+S_d \ . \tag{24}$$

In order to simplify the calculation for diffusion electrons, we have used

$$\int_{E+\varepsilon}^{E_0}dE' f_d(x,\mu,E')\frac{N_A D}{A}\sigma_r(E',E'-E)-\varphi_r f_d\approx\frac{\partial S_{\mathrm{rad}}f_d}{\partial E}+\frac{1}{2}\frac{\partial^2\Omega_r f_d}{\partial E^2} \ . \tag{25}$$

In Appendix A we deduce Eq. (25). Essentially, we consider that the modified CSDA with energy-loss straggling is a good approximation to the transport of the diffusion electrons. Thus we have

$$-\frac{\partial \rho_t f_d}{\partial E}+\mu\frac{\partial f_d}{\partial x}-\frac{1}{2}\frac{\partial^2}{\partial E^2}(\Omega_t f_d)=\frac{N_A D}{A}\int_{4\pi} d\mathbf{u}'[f_d(x,\mu',E)-f_d(x,\mu,E)]\sigma_{\mathrm{MF}}(E,\mathbf{u}\cdot\mathbf{u}') + \frac{N_A}{A}D\int_{E+\varepsilon}^{E_0} dE' f_s(x,\mu,E')\sigma_r(E',E'-E)+S_d \ . \tag{26}$$

Expanding the distribution functions f_s, f_d, and S_d into Legendre polynomials, we have

$$f_s(x,\mu,E)=\sum_{l=0}^{\infty}\frac{2l+1}{4\pi}p_l(\mu)A_l(x,E) \ , \tag{27}$$

$$f_d(x,\mu,E)=\sum_{l=0}^{\infty}\frac{2l+1}{4\pi}p_l(\mu)N_l(x,E) \ , \tag{28}$$

$$S_d(x,\mu,E)=\sum_{l=0}^{m}\frac{2l+1}{4\pi}p_l(\mu)S_l(x,E) \ . \tag{29}$$

For calculation of the distribution function for the forward-directed electrons, we have used two concepts: the partition condition and the narrow-energy-spectrum approximation (NESA) which was proposed in Ref. 23. The main idea of NESA is that if the width of the energy spectrum for a charged particle beam is much narrower than the average energy of the beam, then the interaction cross section between the particle and the atoms in medium in an integral weighted with the charged particle spectrum can be expanded in a Taylor series around the average energy. For the forward-directed electrons, NESA is valid. Using the partition condition, we have

$$C_{f_s}(x,\mu_i,E)=S_d(x,\mu_i,E) \ , \quad i=0,1,\ldots,m \ . \tag{30}$$

Therefore, we have

$$S_l(x,E)=-\varphi_l(E)A_l(x,E)-\sum_{l'=m+1}^{\infty}D_{ll'}\varphi_{l'}A_{l'}(x,E) \ . \tag{31}$$

$m+1$ is the number of large angles selected. $D_{ll'}$ is the partition coefficient, which has already been defined in Ref. 15. Besides, we may use the average directional cosine μ_a instead of the real directional cosine μ in the gradient term in Eq. (23) due to the small-angle property of forward-directed electrons. By definition

$$\mu_a(x)=\frac{\int_0^{E_0}\int_{4\pi}\mu f_s(x,\mu,E)d\mu\,dE}{\int_0^{E_0}\int_{4\pi}f_s(x,\mu,E)d\mu\,dE} \tag{32}$$

$$=\frac{\int_0^{E_0}A_1(x,E)dE}{\int_0^{E_0}A_0(x,E)dE} \ . \tag{33}$$

We can also define an average path length for the forward-directed electrons arriving at point x, $S_a(x)$, and its corresponding average energy of forward-directed electrons $E_a(x)$.

$$S_a(x)=\int_0^x dx'[\mu_a(x')]^{-1} \ , \tag{34}$$

$$E_a(x)=E_0-\int_0^{S_a}L(E,\Delta)dS' \ . \tag{35}$$

In this way, from Eqs. (23) and (27)–(31) we obtain

$$-\frac{\partial}{\partial E}[L(E,\Delta)A_l(x,E)]+\mu_a\frac{\partial A_l}{\partial x}-\frac{1}{2}\frac{\partial^2}{\partial E^2}[\Omega_c A_l(x,E)]+\varphi_r A_l(x,E) = \sum_{l'=m+1}^{\infty}D_{ll'}\varphi_{l'}A_{l'}(x,E)+\delta(x)\delta(E-E_0) \ , \quad l\le m \ , \tag{36}$$

$$-\frac{\partial}{\partial E}[L(E,\Delta)A_l(x,E)]+\mu_a\frac{\partial A_l}{\partial x}-\frac{1}{2}\frac{\partial^2}{\partial E^2}[\Omega_c A_l(x,E)]+\varphi_r A_l(x,E)=-\varphi_l A_l(x,E)+\delta(x)\delta(E-E_0) \ , \quad l>m \ . \tag{37}$$

Following the same calculation in Ref. 15, we have

$$A_l(x,E)=-\sum_{l'=m+1}^{\infty}D_{ll'}A_{l'}(x,E) \ , \quad l\le m \ . \tag{38}$$

Therefore, when we obtain the solution of Eq. (37), we also obtain the solution of Eq. (36). Introducing the Fourier transformation of Eq. (37) and using the NESA approximation, we have

$$\int_{-\infty}^{\infty}e^{ipE}A_l(x,E)U(E)dE\approx U[E_a(x)]B_l(x,p) \ . \tag{39}$$

$B_l(x,p)$ is the Fourier image of $A_l(x,E)$, i.e,

$$B_l(x,p)=\int_{-\infty}^{\infty}e^{ipE}A_l(x,E)dE \ . \tag{40}$$

$U(E)$ is any function for interaction between electron and atom, and Eq. (37) becomes

$$ipL(E_a,\Delta)B_l(x,p)+\mu_a\frac{dB_l}{dx}+\frac{p^2}{2}\Omega_c(E_a)B_l(x,p) + [\varphi_r(E_a)+\varphi_l(E_a)]B_l-\delta(x)e^{ipE_0}=0 \ . \tag{41}$$

Therefore

$$B_l(x,p)=\begin{cases} e^{ip(E_0-\Delta E_c)-\mu_l(x)-\mu_r(x)-p^2w(x)}, & x\geq 0 \\ 0, & x<0, \end{cases} \tag{42}$$

with $\Delta E_c=\int_0^x L(E_a(x'),\Delta)dx'/\mu_a$, then

$$A_l(x,E)=\frac{1}{2\pi}\int_{-\infty}^{\infty} dp\, e^{-ipE+ip(E_0-\Delta E_c)-\mu_l(x)-\mu_r(x)-p^2w(x)}$$

$$=\frac{1}{2\pi}\left[\frac{\pi}{w}\right]^{1/2} e^{-(E-E_a)^2/4w-\mu_l(x)-\mu_r(x)}. \tag{43}$$

Having made a calculation similar to that in Ref. 15, we obtain the distribution function for the forward-directed electrons

$$A_l(x,E)=\frac{1}{2\pi}\left[\frac{\pi}{w}\right]^{1/2} e^{-(E-E_a)^2/4w-\mu_r(x)}\alpha_l(x), \tag{44}$$

$$\alpha_l(x)=\begin{cases} -\sum_{l'=m+1}^{\infty} D_{ll'}e^{-\mu_{l'}(x)}, & l\leq m, \\ e^{-\mu_l(x)}, & l>m, \end{cases} \tag{45}$$

where

$$w(x)=\tfrac{1}{2}\int_0^x \Omega_c(E_a)dx/\mu_a=\tfrac{1}{2}\int_0^S \Omega_c(E_a)dS, \tag{46}$$

$$\mu_l(x)=\int_0^x \varphi_l(E_a)dx/\mu_a=\int_0^S \varphi_l(E_a)dS, \tag{47}$$

$$\mu_r(x)=\int_0^x \varphi_r(E_a)dx/\mu_a=\int_0^S \varphi_r(E_a)dS. \tag{48}$$

Formula (31) for the diffusion electron source is only a formal solution. It is difficult to use formula (31) for a numerical calculation. Fortunately, however, it has been proven that Eq. (31) is identical with the simple formula

$$S_l(x,E)=-\varphi_l(E)A_l(x,E)-A_l\left[\frac{d\ln\alpha_l}{dS}\right], \quad l\leq m. \tag{49}$$

The detailed proof is given in Appendix B.

For the diffusion electrons, the P_n approximation has been used to describe their transport. We have

$$-\frac{\partial\rho_l N_l}{\partial E}+\left[\frac{l+1}{2l+1}\frac{\partial N_{l+1}}{\partial x}+\frac{l}{2l+1}\frac{\partial N_{l-1}}{\partial x}\right]=\frac{1}{2}\frac{\partial^2\Omega_l N_l}{\partial E^2}-\varphi_l N_l+\frac{N_A}{A}D\int_{E+\varepsilon}^{E_0} dE'\, A_l(x,E')\sigma_r(E',E'-E)+S_l,$$

$$l=0,1,\ldots,n. \tag{50}$$

The boundary condition and the initial condition for solving Eq. (50) are the same as those in Ref. 16. Thus, the spherical harmonic moments $N_l(x,E)$ can be obtained.

B. Extension to the oblique incidence

Assume that a conical beam of electrons of energy E_0 is incident upon the semi-infinite homogeneous medium at angle θ_0. The incident geometry is shown in Fig. 2. Since the angular spread of forward-directed electrons is usually small, when satisfying the condition $\pi/2-\theta_0>\theta_m$, the influence of the boundary upon the distribution function of the forward-directed electrons does not exist. For radiation therapy, the incident angle θ_0 often is not very large, and the condition usually is satisfied. This is the case even under the condition $\pi/2-\theta_0<\theta_m$, since only a small portion of the forward-directed electrons can leave the surface directly. The influence of the boundary layer upon the distribution function of forward-directed electrons is still not great. Thus, we will neglect the influence of the boundary on the distribution function of forward-directed electrons. Here θ_m is the smallest large angle among the chosen $m+1$ large-angle directions. Setting an axis X' along the incident direction of the electrons and observing the transport of the forward-directed electrons along X', it may be seen that their transport is the same as that for the normal incidence. In this way, it is possible to derive the distribution function for the forward-directed electrons of oblique incidence from the distribution function for forward-directed electrons of the normal incidence through proper coordinate transformations, and further to obtain the distribution function of diffusion electrons.

In Fig. 2, we set up two axes. One is the axis X', the other is the axis X in the normal direction of surface. In the system (x',μ,E'), the distribution function of the forward-directed electrons does not change. Suppose $\tilde{f}_s$ represents the distribution function of forward-directed electrons and $\tilde{S}_d$ the diffusion electron source in the system $(x',\cos\vartheta,E')$; we have

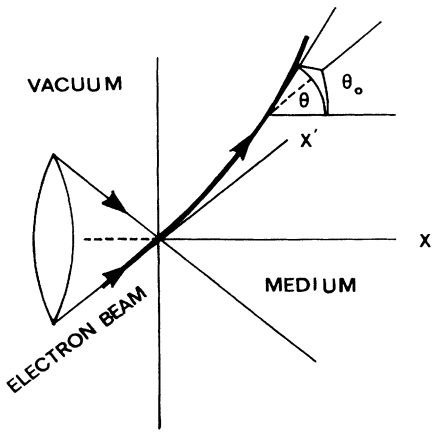

FIG. 2. An illustration for obliquely incident geometry. x, absciss; x', the abscis along the incident direction; θ_0, incident angle; θ, the angle between the x axis and the direction of a forward-directed electron; ϑ, the angle between the x' axis and the direction of the forward-directed electron.

$$\tilde{f}_s(x',\cos\vartheta,E')=\frac{1}{2\pi}\left[\frac{\pi}{w}\right]^{1/2}e^{-(E'-E_a)^2/4w-\mu_r(x')}\times\sum_{l=0}^{\infty}\frac{2l+1}{4\pi}P_l(\cos\vartheta)\alpha_l(x')\ , \tag{51}$$

$$\tilde{S}_d(x',\cos\vartheta,E')=\frac{1}{2\pi}\left[\frac{\pi}{w}\right]^{1/2}e^{-(E'-E_a)^2/4w-\mu_r(x')}\times\sum_{l=0}^{m}\frac{2l+1}{4\pi}P_l(\cos\vartheta)S_l(x')\ . \tag{52}$$

When the coordinate system (x',ϑ,E') is transformed into coordinate (x,θ,E), we have the following transformation:

$$x'=x/\cos\theta_0\ ,$$
$$E'=E\ , \tag{53}$$
$$\cos\vartheta=\cos\theta_0\cos\theta+\sin\theta_0\sin\theta\cos(\varphi-\varphi_0)\ .$$

Under the geometric condition of conical symmetry, the distribution function of the forward-directed electrons should be average over azimuth angle φ, i.e.,

$$f_s(x,\mu,E)=\int_0^{2\pi}\tilde{f}_s(x',\cos\vartheta,E)d\varphi/2\pi=\sum_{l=0}^{\infty}\frac{2l+1}{4\pi}P_l(\mu)A_l(x,E)\ . \tag{54}$$

Note that the average projection distance of the forward-directed electrons along the axis X' is

$$x'=\int_0^{S'}\mu_a(s')ds'=\int_0^{S'}\alpha_1(s')ds'/\alpha_0(s')\ . \tag{55}$$

Thus

$$f_s(x,\mu,E)=\frac{1}{2\pi}\left[\frac{\pi}{w}\right]^{1/2}e^{-(E-E_a)^2/4w}\times\sum_{l=0}^{\infty}\frac{2l+1}{8\pi^2}\alpha_l(x')e^{-\mu_r(x')}\int_0^{2\pi}P_l(\cos\vartheta)d\varphi\ . \tag{56}$$

Using the addition theorem of Legendre polynomials, we have

$$A_l(x,E)=(4\pi w)^{-1/2}e^{-(E-E_a)^2/4w-\mu_r(x')}P_l(\mu_0)\alpha_l(x')\ ,$$
$$\mu_0=\cos\theta_0\ , \tag{57}$$

$$S_l(x,E)=P_l(\mu_0)S_l(x',E)\ . \tag{58}$$

Having obtained $S_l(x,E)$, we can use Eq. (50) and its boundary and initial conditions to calculate the spherical harmonic moments of the diffusion electrons $N_l(x,E)$.

C. The secondary-electron transport

To calculate the secondary-electron transport, we have made some simplifications. (1) Only such secondary electrons directly produced by primary electrons have been considered in our calculation. Generally, these secondary electrons are the main part of all secondary electrons. (2) CSDA has been used to describe their transport. (3) Because the angular distribution of secondary electrons is rather isotropic, P_n approximation has been used to calculate the spherical harmonic moments for the secondary electrons.

When a primary electron collides with a free electron, from the momentum and energy conservation laws, the direction of motion of the recoil electron, $\mathbf{u}'$, is governed by the relation

$$\mathbf{u}\cdot\mathbf{u}'=\left[\frac{T(E+2m_0c^2)}{E(T+2m_0c^2)}\right]^{1/2}\ . \tag{59}$$

T is the energy transferred to the secondary electron. E is the energy of the primary electron. Thus the secondary-electron source $\tilde{S}(x,\mu,E)$ produced by primary electrons is

$$\tilde{S}(x,\mu,E)=\frac{N_AZ}{A}D\int_{4\pi}d\mathbf{u}'\int_{2E}^{E_0}dE'\,\sigma_M(E',E)\frac{1}{2\pi}\delta\left[\mathbf{u}\cdot\mathbf{u}'-\left[\frac{E(E'+2m_0c^2)}{E'(E+2m_0c^2)}\right]^{1/2}\right]f(x,\mu',E')\ . \tag{60}$$

Expanding $\tilde{S}(x,\mu,E)$ into a Legendre polynomial series, we have

$$\tilde{S}(x,\mu,E)=\sum_{n=0}^{\infty}\frac{2n+1}{4\pi}P_n(\mu)\tilde{S}_n(x,E)\ , \tag{61}$$

where

$$\tilde{S}_n(x,E)=\int_{2E}^{E_0}dE'\frac{N_AZ}{A}D\sigma_M(E',E)P_n\left[\frac{E(E'+2m_0c^2)}{E'(E+2m_0c^2)}\right]^{1/2}f_n(x,E)\ . \tag{62}$$

We know that the NESA is valid for $f_n(x,E)$, the nth spherical harmonic moment of the primary electrons; therefore we have

$$f_n(x,E)\approx\left[\alpha_n(x)+\int_0^{E_0}N_n(x,E')dE'\right]\delta(E-E_a)\ . \tag{63}$$

Inserting Eq. (63) into Eq. (62), we have

$$\tilde{S}_n(x,E)=\frac{N_A Z}{A}D\sigma_M(E_a,E)P_n\left[\frac{E(E_a+2m_0c^2)}{E_a(E+2m_0c^2)}\right]^{1/2}\left[\alpha_n(x)+\int_0^{E_0}N_n(x,E')dE'\right] . \tag{64}$$

From $\tilde{S}_n$, the P_3 approximation can be used to calculate the secondary-electron transport, and we have

$$-\frac{\partial\rho_t\tilde{N}_n}{\partial E}+\left[\frac{n+1}{2n+1}\right]\frac{\partial\tilde{N}_{n+1}}{\partial x}+\left[\frac{n}{2n+1}\right]\frac{\partial\tilde{N}_{n-1}}{\partial x}=-\varphi_n\tilde{N}_n+\tilde{S}_n \ , \quad n\le 3 . \tag{65}$$

Using the same boundary and initial conditions, we can obtain the spherical harmonic moments for secondary electrons, $\tilde{N}_n(x,E)$.

IV. CALCULATIONAL RESULTS

By applying the above extended form of the bipartition theory for the electron transport, we have completed transport calculations for electrons with energy from 1 to 50 MeV normally and obliquely incident on water. The electron-energy deposition, the electron charge distribution, and the angular distribution of electrons at various depths have been calculated. Moreover, a comparison between the bipartition model and existing experimental and Monte Carlo data has been made. The following are our main computational results.

A. The choice of calculation parameters

In accordance with the electron bipartition transport theory generalized above, we compiled a program MONKEY.RT, which is specially developed for calculation of electron transport in the above-mentioned energy range in water or soft tissues of the human body. Because of the high efficiency of the bipartition theory, in a standard calculation, we would rather choose the calculation parameters which, though more time consuming, will give higher precision. The calculations also showed that, even when a more economical calculation was selected, the calculational precision was only weakly affected even though much time was saved. This fact shows that the bipartition theory does have a potential to allow accurate real-time calculations.

In a standard calculation, the number of terms in the Legendre polynomial series of the forward-directed electron distribution function, M_L, is usually chosen as 200. The number of the selected large-angle directions for diffusion electrons, M_A, is 5. The largest penetration depth is $1.5r_0$, where r_0 is the CSDA range of the incident electrons. The depth interval has been equally divided into N_X segments, $N_X=150$. The electron-energy interval has been divided into N_E segments, $N_E=100$. The division of the electron-energy interval is not uniform, but it guarantees equal relative residual range segments. Such energy intervals are more suitable for solving the hyperbolic equation for diffusion electrons. For the diffusion electrons we generally use P_9 approximation, i.e., $N_{PL}=9$. N_{PL} is the order of P_n approximation. For the transport of secondary electrons, we use P_3 approximation.

Some special considerations have been given to the choice of large-angle directions. In earlier calculations, the directional cosine corresponding to the smallest large angle is usually between 0.2 and 0.5, corresponding to 80°–60°. While calculating the transport of the electrons of several tens of megaelectron volts in water, though the bremsstrahlung does not contribute greatly to stopping power, it does contribute greatly to the straggling process. This means that the electron spectrum is rapidly broadened at large depths and this fact restricts the use of the NESA. To avoid such a situation, we have chosen a large cosine of the smallest large-angle so as to move more scattered forward-directed electrons to the diffusion electron group. The result is that, when the NESA is no longer valid, the number of the forward-directed electrons is low, and as a result, the problem brought about by the NESA and the Fokker-Planck approximation is small. In the present calculation, the cosine of the smallest large angle is 0.7.

B. Energy deposition

For radiotherapy applications we are most interested in the electron-energy deposition in water. Besides the interest in normally incident electron beams, there is also a clinical interest in the energy deposition produced by an electron beam obliquely incident on water. In the present calculation, a systematic calculation for the electron-energy range from 1 to 50 MeV has been made and the results have been compared with existing experimental and Monte Carlo data.

The electron-energy deposition in the bipartition model consists of three parts: the contributions from the forward-directed electrons, diffusion electrons, and the secondary electrons produced by primary electrons consisting of the forward-directed electrons and diffusion electrons:

$$D_E=D_p+D_s \ . \tag{66}$$

D_E is the total energy deposition, D_p is the energy deposition by primary electrons, and D_s is the energy deposition of secondary electrons. Obviously

$$D_p=\int_0^{E_0}[A_0(x,E)+N_0(x,E)]L(E,\Delta)dE \ , \tag{67}$$

$$D_s=\int_0^{E_0/2}\tilde{N}_0(x,E)L(E,E/2)dE \ , \tag{68}$$

where Δ is $0.02E_0$ in our calculation. E_0 is initial energy

of incident electrons. Figure 3 shows a comparison of energy deposition of $30m_0c^2$ electron in water by using the bipartition model with the moment method.[2] The energy deposition decrease near the surface is due to the escape of secondary electrons from the surface. This effect is not reflected in the moment method. For our energy deposition a considerable amount of electrons can penetrate deeper than the CSDA range due to the effect of energy-loss straggling, but the moment method cannot treat this important problem. The energy depositions for 10-, 20-, and 40-MeV electron beams are shown in Figs. 4, 5, and 6, respectively, and compare them with the experimental data in Refs. 24 and 25. The comparison shows that the extended bipartition model can well calculate the energy deposition for high-energy electrons in water. Figure 7 shows the energy depositions by obliquely incident electrons at the angles of 0°, 15°, 30°. It is important that, even for the incident electron with 15°, the change of energy deposition should not be neglectible for radiation therapy. Therefore, the correction of dose distribution for obliquely incident electron beams in treatment planning must be carefully considered.

C. Charge distribution

The charge distribution produced by electron beam in an insulator is of some interest in radiation effects. The charge distribution in a solid, $C(x)$, not only depends on the primary-electron transport, but also depends on secondary-electron transport. In order to calculate the charge distribution we assume there is a vacancy at the point where a secondary electron is released from an atom and the charge distribution is simply the spatial distribution of electrons with zero energy. Thus, we have

$$C(x)=N_0(x,E\to 0)+\tilde{N}_0(x,E\to 0)-\int_{\Delta}^{E_0}dE'\int_{\Delta}^{E'/2}dT\,\frac{N_A Z}{A}D[A_0(x,E')+N_0(x,E')]\sigma_M(E',T)\ . \tag{69}$$

We have calculated the charge distribution for 20-MeV electrons, and compared with the results obtained by the Monte Carlo method. Figure 8 shows the computation results. The agreement between our results and the Monte Carlo results is fairly good, although the results of Monte Carlo show a slightly deeper penetration.[26]

D. The angular distribution

In order to understand the electron transport process better and check the extended model in detail, we have also calculated the electron angular distribution at depth. By definition, the angular distribution of the fluence is

$$A(x,\mu)=\sum_{l=0}^{100}\frac{2l+1}{4\pi}P_l(\mu)\alpha_l(x)+\sum_{l=0}^{9}\frac{2l+1}{4\pi}P_l(\mu)\int_0^{E_0}N_l(x,E)dE+\sum_{l=0}^{3}\frac{2l+1}{4\pi}P_l(\mu)\int_0^{E_0}\tilde{N}_l(x,E)dE\ . \tag{70}$$

Figure 9 shows the angular distribution at depth $x=0.07$, 0.017, 0.37, and 0.77 for 10-MeV electrons in water. The corresponding results obtained by the Monte Carlo method are also given in the same figure.[14] It is shown that the agreement between both calculations is quite good, except possibly for the largest depth.

The computational results of the current angular distribution at $x=0.62$ for 10-MeV electrons in carbon are

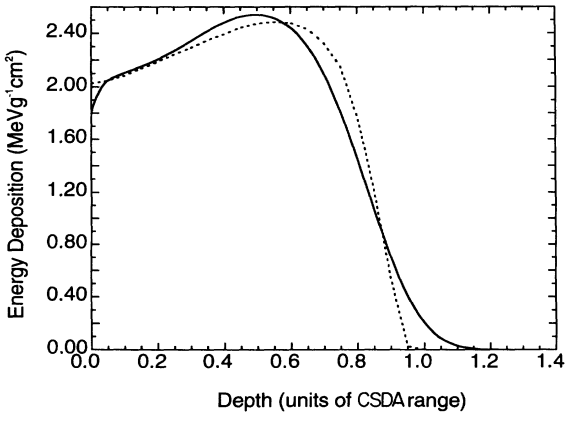

FIG. 3. The energy deposition for $30m_0c^2$ electrons in water. The solid line shows the computational results given by the extended bipartition model. The dashed line shows the Kessaris data by using the moment method (Ref. 2).

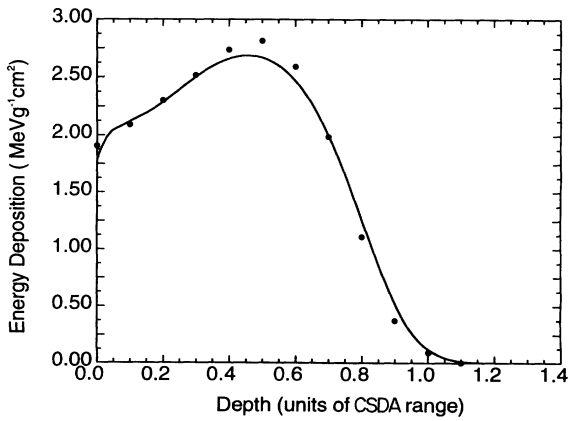

FIG. 4. The energy deposition for 10-MeV electrons in water. The solid line shows the results obtained by using the extended bipartition model. The solid points show the experimental data (Ref. 25).

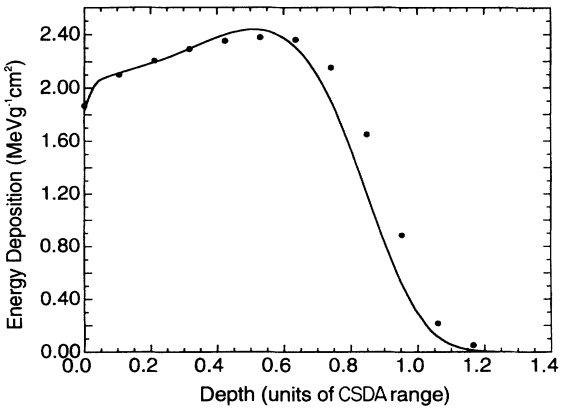

FIG. 5. The energy deposition for 20-MeV electrons in water. The solid line shows the results obtained by using the extended bipartition model. The solid points show the experimental data (Ref. 25).

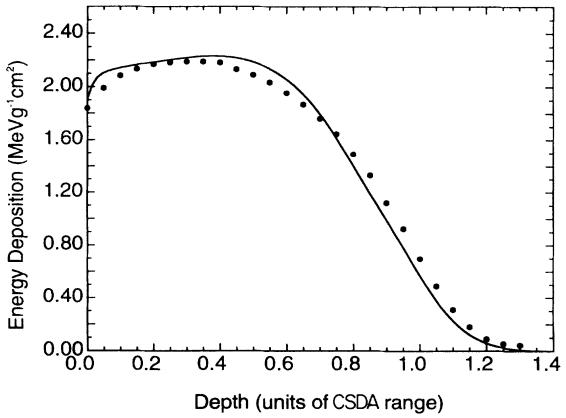

FIG. 6. The energy deposition for 40-MeV electrons in water. The solid line shows the results obtained by using the extended bipartition model. The solid points show the experimental data (Ref. 25).

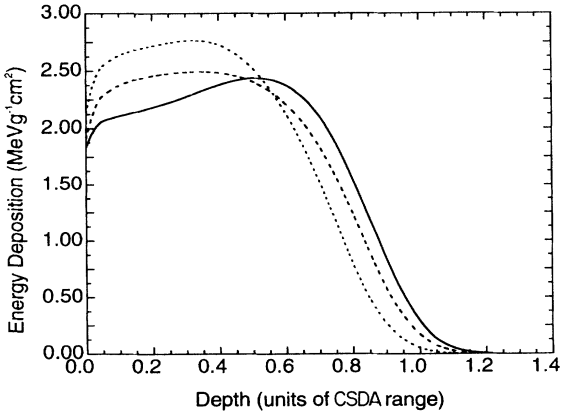

FIG. 7. The energy deposition for 20-MeV electrons obliquely incident into water. The incident angles are 0°, 15°, 30°.

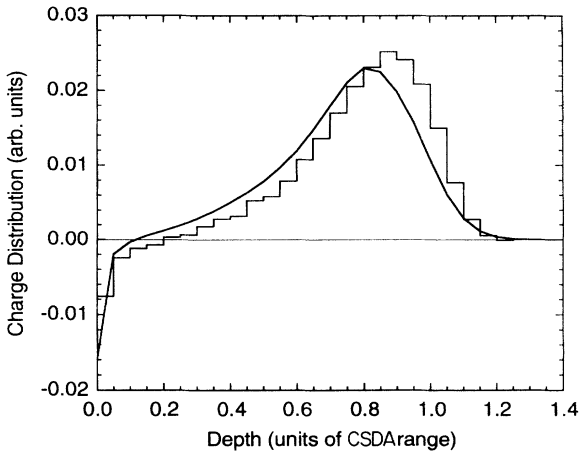

FIG. 8. The charge distribution for 20-MeV electrons in water. The solid line shows the results obtained by using the extended bipartition model. The histogram shows the data given by the Monte Carlo method (Ref. 26).

given in Fig. 10. The experimental angular distributions $J(x,\mu)$ measured by Roos and others are given in the same figure. By definition, $J(x,\mu)$ is

$$J(x,\mu)=\mu A(x,\mu) . \tag{71}$$

Obviously, only the extended bipartition model can reach good agreement with the experimental data.[27–29]

E. Calculation efficiency

In a standard calculation, it takes only 2 min to complete a transport calculation on an HP-900-750 computer, when the calculation parameters are taken from the above-mentioned numerical parameters. If we choose a set of more economical parameters, for example, we can take $M_L=100$, $N_X=60$, $N_E=40$, $N_{PL}=5$, then 10 s would be sufficient for a calculation with minimal loss of calculation precision. Figure 11 shows the energy deposi-

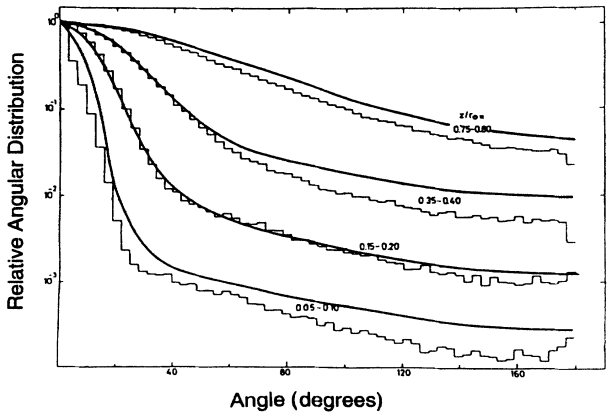

FIG. 9. The relative angular distribution of 10-MeV electrons in water at different depths. The solid line shows the electron angular distribution at $x=0.07$, 0.17, 0.37, and 0.77. The histogram shows the electron angular distribution resulted within 0.05–0.10, 0.15–0.20, 0.35–0.40, and 0.75–0.80 obtained by using a Monte Carlo simulation (Ref. 14).

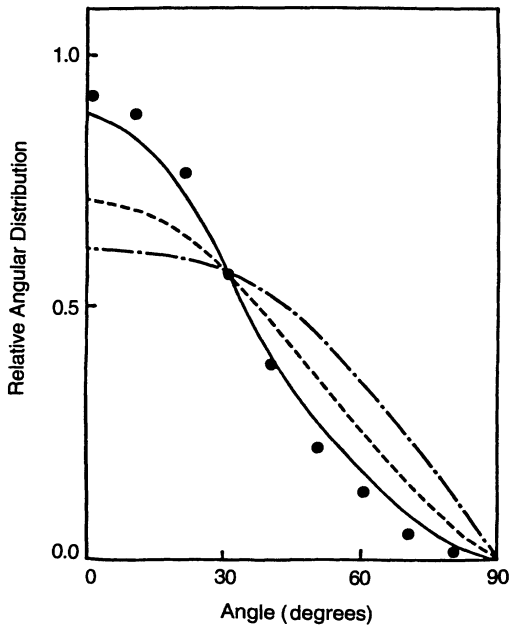

FIG. 10. The relative angular distribution of 10-MeV electrons passing through graphite with 3.84 g cm^{-2} thickness. The solid line shows the results obtained by using the extended bipartition model. Circles show the experimental data given in Ref. 27. The dash-dotted line shows the results obtained by using the Bethe theory presented in Ref. 28. The dashed line shows the results obtained by a modified Bethe theory (Ref. 29).

tion of 10-MeV electrons in water. The results when standard parameters are used are given by the solid line, and the results with the economical parameters stated above are indicated by the dotted line. It can be seen that there are only minor differences between them indicating that the bipartition model is a highly effective calculational method.

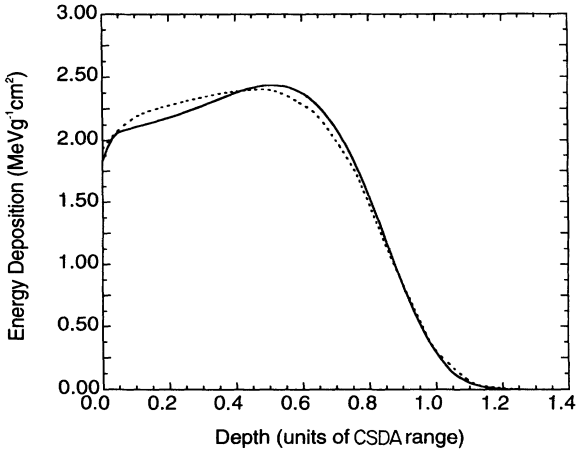

FIG. 11. A comparison between two curves corresponding to the different computation parameters. The solid line shows the computational results corresponding to the parameters $M_L=200$, $N_X=150$, $N_E=100$, $N_{PL}=9$, and the computation real time is 120 s at an HP-900-750 computer. The dotted line shows the computational results corresponding to the parameters $M_L=50$, $N_X=60$, $N_E=40$, $N_{PL}=5$, and the computation real time is 10 s at the same computer.

V. DISCUSSION AND CONCLUSION

How does the fundamental interactions between electrons and atoms in a medium influence the transport? The so-called fundamental interaction processes here are the following interactions: elastic scattering, bremsstrahlung, secondary-electron production, and inelastic scattering. Owing to the fact that the influence of inelastic scattering does not reflect through individual interaction of electrons with atoms in media, but do reflect through nonstochastic energy loss (CSDA) and stochastic energy loss (CSDA with energy-loss straggling), we first investigate the simplest CSDA solution without elastic scattering and bremsstrahlung. In that case we have a degradation form of Eq. (19),

$$-\frac{\partial \rho_c f}{\partial E}+\mu\frac{\partial f}{\partial x}-\frac{1}{2}\frac{\partial^2\Omega_c f}{\partial E^2}=\delta(x)\delta(1-\mu)\delta(E-E_0)/2\pi\ . \tag{72}$$

Using the NESA, it is easy to obtain an approximate solution. Let

$$f=\delta(1-\mu)f_0(x,E)/4\pi\ .$$

Therefore

$$-\frac{\partial \rho_c f_0}{\partial E}+\frac{\partial f_0}{\partial x}-\frac{1}{2}\frac{\partial^2\Omega_c f_0}{\partial E^2}=2\delta(x)\delta(E-E_0)$$

and obviously

$$f_0=\frac{1}{\pi}\left[\frac{\pi}{w(x)}\right]^{1/2}e^{-(E-E_a)^2/4w}\ . \tag{73}$$

Correspondingly, the energy deposition is

$$D(x)=\int_0^{E_0}dE\,\rho_c(E)\int_{4\pi}d\mathbf{u}\,f(x,\mu,E)$$
$$=\int_0^{E_0}dE\,\rho_c(E)\frac{1}{2\pi}\left[\frac{\pi}{w}\right]^{1/2}e^{-(E-E_a)^2/4w}\approx\rho_c(E_a)\ . \tag{74}$$

If we consider the influence of elastic scattering, Eq. (19) becomes as follows, without the straggling term,

$$-\frac{\partial \rho_t f}{\partial E}+\mu\frac{\partial f}{\partial x}=C(f)+\delta(x)\delta(1-\mu)\delta(E-E_0)/2\pi\ . \tag{75}$$

This is Lewis' electron transport equation and we can obtain an approximate solution to the equation by using the earlier bipartition model.[15] Finally, we have the present solution for which the bremsstrahlung, secondary electron, and energy-loss straggling have been included. Let us make a comparison among them in Fig. 12 for the energy deposition of 1-MeV electrons and in Fig. 13 for the energy deposition of 30-MeV electrons. From the comparison we may see that the CSDA and elastic scattering are important for transport of electrons with energy range below 1 MeV. However, CSDA, elastic scatting, bremsstrahlung, and energy-loss straggling together make

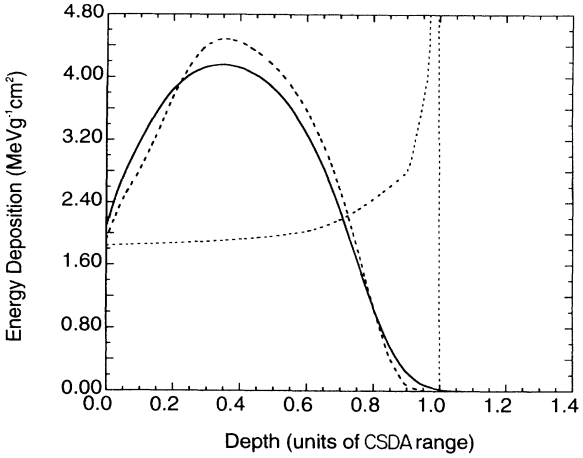

FIG. 12. A comparison among three energy deposition curves for 1-MeV electrons in water, corresponding to different approximations. The solid line shows the results obtained by using the extended bipartition model that involves influences of energy-loss straggling, secondary-electron creation, and bremsstrahlung recoil electrons on transport. The dashed line shows the results given by the earlier bipartition model in which only CSDA and elastic scattering are involved. The short-dashed line shows the solution of Eq. (72) for which only CSDA without elastic scattering is considered.

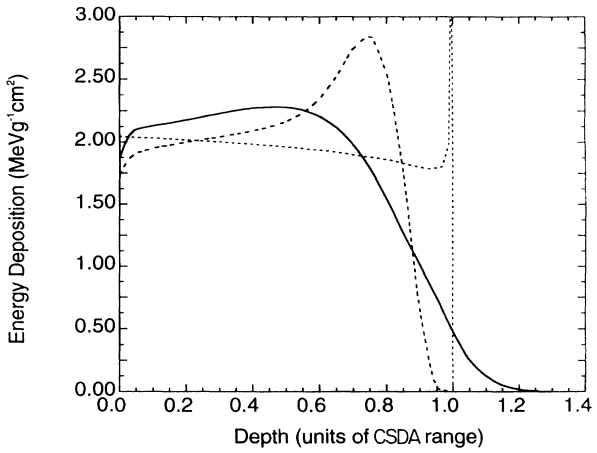

FIG. 13. A comparison among three energy deposition curves for 30-MeV electrons in water, corresponding to different approximations. The solid line shows the results obtained by using the extended bipartition model that involves influences of energy-loss straggling, secondary-electron creation, and bremsstrahlung recoil electrons on electron transport. The dashed line shows the results given by the earlier bipartition model in which only CSDA and elastic scattering are involved. The short-dashed line shows the solution of Eq. (72) for which only CSDA without elastic scattering is considered.

gether make important contributions to total energy deposition for the electron-energy range from 1 to 50 MeV. Comparably speaking, the secondary-electron transport influences the global behavior of electron transport to a smaller extension.

The present type of bipartition model has given results that generally agree with those of available experimental data and Monte Carlo calculations. Furthermore, its calculation efficiency is very much higher than that of the latter and also other numerical methods. The difference between the results of the bipartition model and those of the experiment and the Monte Carlo method is generally only a few percent. Yet, in view of the needs of medical physics, further increase of the precision is desirable. A major reason for the differences is that the contribution from bremsstrahlung to the energy deposition has so far been disregarded. In addition, a method which can furnish a description of forward-directed electrons better than the Fokker-Planck approximation might also be valuable.

ACKNOWLEDGMENTS

The authors are grateful to P. Andreo for instructive discussions and supplying the Monte Carlo data. Thanks are also due to Bengt K. Lind, Patric Kallman, and Shi Liu for their help with the use of the computer. The research has been supported in part by the Natural Science Foundation of China and the Swedish Cancer Society.

APPENDIX A

We have made use of the fact that

$$\int_E^{E_0}\frac{N_A D}{A}\sigma_r(E',E'-E)f_d(x,\mu,E')dE'-f_d(x,\mu,E)\int_0^E\frac{N_A D}{A}\sigma_r(E,T)dT$$
$$=\frac{1}{2\pi}\int_{-\infty}^{\infty}e^{-ipE}dp\int_{-\infty}^{\infty}dE\,e^{ipE}\left[\int_E^{E_0}\frac{N_A D}{A}\sigma_r(E',E'-E)f_d(x,\mu,E')dE'-f_d(x,\mu,E)\int_0^E\frac{N_A D}{A}\sigma_r(E,T)dT\right]. \tag{A1}$$

We extend the definition domain for the function $f_d(x,\mu,E)$ as follows:

$$f_d(x,\mu,E)=\begin{cases}f_d(x,\mu,E)\ , & 0\le E\le E_0\ ,\\ 0\ , & E<0,E>E_0\ .\end{cases} \tag{A2}$$

Correspondingly, the definition domain for the function $\sigma_r(E,T)$ will be analytically extended. Thus

$$f_d^*(x,\mu,p)=\int_{-\infty}^{\infty}f_d(x,\mu,E)e^{ipE}dE=\int_0^{E_0}f_d(x,\mu,E)e^{ipE}dE\ . \tag{A3}$$

Exchanging the order of integral in Eq. (A1), we have

$$\int_0^{E_0} dE\, e^{ipE} \int_E^{E_0} dE' f_d(x,\mu,E') \frac{N_A D}{A} \sigma_r(E',E'-E) dE' = \int_0^{E_0} dE' f_d(x,\mu,E') e^{ipE'} \int_0^{E'} dT \frac{N_A D}{A} \sigma_r(E',T) e^{-ipT} . \quad \text{(A4)}$$

Thus, we have

$$\begin{aligned} &\int_E^{E_0} dE' f_d(x,\mu,E') \frac{N_A D}{A} \sigma_r(E',E'-E) - f_d(x,\mu,E) \int_0^{E_0} dT \frac{N_A D}{A} \sigma_r(E,T) dT \\ &\quad = \frac{-1}{2\pi} \int_{-\infty}^{\infty} e^{-ipE} dp \int_0^{E_0} dE\, f_d(x,\mu,E) e^{ipE} \int_0^{E} dT \frac{N_A}{A} \sigma_r(E,T)(1-e^{-ipT}) \\ &\quad \approx \frac{-1}{2\pi} \int_{-\infty}^{\infty} e^{-ipE} dp \int_0^{E_0} dE\, f_d(x,\mu,E)(ipS_{\text{rad}} + p^2 \Omega_r/2) e^{ipE} \\ &\quad = \frac{\partial S_{\text{rad}} f_d(x,\mu,E)}{\partial E} + \frac{1}{2} \frac{\partial^2}{\partial E^2} [\Omega_r f_d(x,\mu,E)] . \end{aligned} \quad \text{(A5)}$$

APPENDIX B

We have Eq. (36), then

$$-\sum_{l'=m+1}^{\infty} D_{ll'} \varphi_{l'} A_{l'} = \frac{\partial}{\partial E} [L(E,\Delta) A_l(x,E)] - \mu_a \frac{\partial A_l}{\partial x} + \frac{1}{2} \frac{\partial^2}{\partial E^2} [\Omega_c A_l(x,E)] - \varphi_r A_l . \quad \text{(B1)}$$

Adopting the same method as that to solve Eq. (39), we have

$$-\sum_{l'=m+1}^{\infty} D_{ll'} \varphi_{l'} A_{l'} = L(E_a,\Delta) \frac{\partial A_l}{\partial E} - \mu_a \frac{\partial A_l}{\partial x} + \tfrac{1}{2} \Omega_c(E_a) \frac{\partial^2 A_l}{\partial E^2} - \varphi_r A_l . \quad \text{(B2)}$$

By differentiation of A_l, we have

$$\frac{\partial A_l}{\partial E} = \left[-\frac{E-E_a}{2w} \right] A_l(x,E) , \quad \text{(B3)}$$

$$\frac{\partial^2 A_l}{\partial E^2} = \left[-\frac{(E-E_a)^2 - 2w}{4w^2} \right] A_l(x,E) , \quad \text{(B4)}$$

$$\frac{\partial A_l}{\partial x} = \left[-\frac{1}{2w} \frac{dw}{dx} + \left[\frac{E-E_a}{2w} \frac{dE_a}{dx} - \frac{(E-E_a)^2}{w^2} \frac{dw}{dx} - \frac{d\mu_r}{dx} \right] + \frac{d\ln\alpha_l}{dx} \right] A_l(x,E) . \quad \text{(B5)}$$

Inserting the following equations into Eq. (B2),

$$\frac{dw}{dx} = \frac{\Omega_c}{2\mu_a} , \quad \text{(B6)}$$

$$\frac{dE_a}{dx} = -L \frac{1}{\mu_a} , \quad \text{(B7)}$$

$$\frac{d\mu_r}{dx} = \frac{\varphi_r}{\mu_a} , \quad \text{(B8)}$$

we obtain

$$S_l(x,E) = A_l(x,E) \left[-\varphi_l - \frac{d\ln\alpha_l}{dS} \right] . \quad \text{(B9)}$$

[1] L. V. Spencer, Phys. Rev. **98**, 1579 (1955).
[2] N. D. Kessaris, Radiat. Res. **23**, 630 (1964).
[3] E. Fermi, as cited by B. Rossi and K. I. Greisen, Rev. Mod. Phys. **13**, 265 (1941).
[4] L. Eyges, Phys. Rev. **74**, 1534 (1948).
[5] A. Brahme (unpublished).
[6] D. Jette, Med. Phys. **12**, 178 (1985).
[7] K. R. Hogstrom, M. D. Mills, and P. R. Almond, Phys. Med. Biol. **26**, 445 (1981).
[8] A. Brahme, I. Lax, and P. Andreo, Acta Radiol. Oncol. **21**, 147 (1981).
[9] M. C. Cordaro and M. S. Zucker, Nucl. Sci. Eng. **45**, 107

(1971).
[10]H. Huizenga and P. R. M. Storchi, Phys. Med. Biol. **34**, 1371 (1989).
[11]M. J. Berger and S. M. Seltzer (unpublished).
[12]J. A. Halbleib and W. H. Vandevender, Nucl. Sci. Eng. **57**, 94 (1975).
[13]W. R. Nelson, H. Hirayama, and D. W. O. Rogers (unpublished).
[14]P. Andreo and A. Brahme, Radiat. Res. **100**, 16 (1984).
[15]Luo Zhengming, Phys. Rev. B **32**, 812 (1985).
[16]Luo Zhengming, Phys. Rev B **32**, 824 (1985).
[17]H. A. Bethe, Ann. Phys. (Leipzig) **5**, 325 (1930).
[18]W. Heitler, *The Quantum Theory of Radiation,* 2nd ed. (Oxford University Press, London, 1936).
[19]S. M. Seltzer and M. J. Berger, Int. J. Appl. Radiat. Isot. **33**, 1219 (1982).
[20]H. A. Bethe and J. Ashkin, in *Passage of Radiation Through Matter,* Experimental Nuclear Physics Vol. 1, edited by E. Segrè (Wiley, New York, 1960).
[21]W. A. McKinley and H. Feshbach, Phys. Rev. **74**, 1759 (1948).
[22]G. Moliere, Z. Naturforsch. A **2**, 133 (1947); **3**, 78 (1948).
[23]Luo Zhengming, Acta Phys. Sin. **31**, 1166 (1982).
[24]A. Brahme and H. Svensson, Acta Radiol. Oncol. **18**, 1244 (1979).
[25]A. Brahme, T. Kraepelien, and H. Svensson, Acta Radiol. Oncol. **19**, 305 (1980).
[26]P. Andreo (private communication).
[27]H. Roos, P. Drepper, and D. Harder, in *Proceedings of the Fourth Symposium on Microdosimetry, Verbania, Pallanza, Italy,* edited by J. Booz *et al.* (Commission of the European Communities, Luxenbourg, 1974), p. 779.
[28]H. A. Bethe, M. E. Rose, and L. P. Smith, Proc. Am. Philos. Soc. **78**, 573 (1938).
[29]D. Harder, *Dosimetrie und Strahlenschutz* (Thieme, Stuttgart, 1974), p. 102.